DOI 10.1007/s11062-023-09930-6
Neurophysiology, Vol. 54, Nos. 1–2, January, 2022

Modes of Operation of the Endoplasmic Reticulum Ca^{2+} Transport Systems in Neurons: Insights from the Compartmental Models

E. È. Saftenku[1]

Received March 31, 2022

In neurons, the endoplasmic reticulum (ER) modulates elevations of the cytosolic free Ca^{2+} concentration ($[Ca^{2+}]_i$) in response to extracellular stimulation by accumulating Ca^{2+} via the sarcoplasmic/endoplasmic reticulum Ca^{2+}-ATPases (SERCAs) or by releasing Ca^{2+} via the ER Ca^{2+} channels. SERCA inhibitors are often used as a tool for investigating the contribution from ER Ca^{2+} transport to the $[Ca^{2+}]_i$ dynamics. The respective effects on Ca^{2+} responses in different neurons are characterized by a large diversity. However, the factors that determine this diversity have not been completely understood. Using a simple two-compartment model of the Ca^{2+} dynamics, we showed that changes in the density and relative contribution of ryanodine receptors and SERCA pumps, stimulation conditions, and dye concentration are sufficient to reproduce either smoothly graded, or non-linearly graded, or all-or-non ER Ca^{2+} release and many effects of SERCA inhibitors on the Ca^{2+} transients observed in different neurons. Here, we have redefined main modes of the net ER Ca^{2+} transport (net Ca^{2+} uptake, non-regenerative Ca^{2+} release, and regenerative Ca^{2+} release) and showed that these modes are completely determined by the interplay between Ca^{2+} fluxes and the Ca^{2+} buffering rate. Our simulations demonstrate that low-gain models of Ca^{2+}-induced calcium release (CICR) do not require any counteracting termination mechanism for the release termination. The simulations also suggested that Ca^{2+} transients in some neurons may be modestly amplified by regenerative CICR, which is, nonetheless, graded and self-limiting due to CICR termination mechanisms, such as store depletion and/or Ca^{2+}-dependent inactivation of ryanodine receptors. However, a spatially homogeneous model fails to reproduce both smoothly graded and high-gain CICR.

Keywords: Ca^{2+}-induced calcium release, neurons, endoplasmic reticulum, calcium dynamics, modeling.

INTRODUCTION

Ca^{2+} is a universal signaling agent involved in the regulation of most neuronal functions [1]. The endoplasmic reticulum (ER) in neurons and its specialized counterpart in muscle cells, the sarcoplasmic reticulum (SR), accumulate Ca^{2+} via the SR and ER Ca^{2+}-ATPases (SERCAs) and release Ca^{2+} into the cytosol via Ca^{2+}-activated calcium channels of the store membrane. In contrast to Ca^{2+} transport by the SR in cardiac muscle cells, Ca^{2+} release from the neuronal ER is characterized by a wide diversity [2]. The mechanisms underlying this diversity have been poorly understood. During neuronal depolarization, the ER may act as a Ca^{2+} source or as a sink [3]. The release of Ca^{2+} from the ER in neurons may be smoothly graded [4], non-linearly graded [5], or an all-or-none event [6]. In some neurons, Ca^{2+} release operates in a low-gain regime, i.e., the amount of Ca^{2+} released from the ER is lower than the amount of Ca^{2+}, which enters the cell through plasma membrane (PM) channels (gain < 1.0). In some other types of neurons, a 10-fold amplification of the Ca^{2+} transient may, however, be achieved [2, 5]. There are two families of Ca^{2+} release channels in neurons, namely Ca^{2+}-activated ryanodine receptors (RyRs) and inositol 1,4,5-trisphosphate (IP_3) receptors activated by both IP_3 and Ca^{2+} [2]. In this paper, the IP_3-induced calcium release will not be analyzed.

The contribution of Ca^{2+} transport by the ER to $[Ca^{2+}]_i$ transients is often studied with the use of inhibitors of SERCAs, thapsigargin (TG) or cyclopiazonic acid (CPA). Prolonged treatment of

[1] Bogomolets Institute of Physiology, National Academy of Sciences of Ukraine, Kyiv, Ukraine.
Correspondence should be addressed to E. È. Saftenku (e-mail: esaft@biph.kiev.ua).

different neurons with SERCA inhibitors results in the elimination of ER Ca^{2+} transport. Calcium transients in the spines, dendrites, presynaptic terminals, and somata of some neuronal subtypes do not demonstrate any significant changes in the amplitude but show a slower decay after such treatment [7, 8]. In other neuronal subtypes, SERCA inhibitors decrease the amplitude of $[Ca^{2+}]_i$ transients and may accelerate [9, 10], exert no influence on [11−13], or slow the decay [13, 14] of these transients.

Spatially homogeneous compartmental models of Ca^{2+} dynamics are thought to be an adequate tool for interpreting depolarization-induced fluorescence signals in the dendritic segments and axonal boutons of neurons [15, 16]. In previous works [17, 18], three modes of Ca^{2+}-induced calcium release (CICR) in bullfrog sympathetic neurons were described. These modes, however, were proposed for a condition of the constant free Ca^{2+} concentration in the ER ($[Ca^{2+}]_{ER}$); the authors did not explicitly model the counteracting termination mechanisms and buffers. In our study, we have tested determinants of the modes of net ER Ca^{2+} transport, which accounted for a variety of the action of SERCA inhibitors on Ca^{2+} transients in different neurons.

METHODS

In our model, a neural cell was represented by a cylinder with a diameter of 0.76 μm (that corresponds to the diameters of dendritic endings in cerebellar granule cells, GrCs [10], small dendrites of hippocampal CA_1 pyramidal neurons [8], or small presynaptic boutons [19]). The model consists of two compartments, the cytosol and the ER. The fractional cytosolic volume was set at 83.3%. This value was selected according to an assumption that the ratio of both ER vs. cytosolic volumes and mitochondrial vs. cytosolic volumes is 0.1 [18, 20]. Mitochondrial Ca^{2+} transport was not included in the model, since its contribution to the Ca^{2+} dynamics was found to be negligible at submicromolar values of $[Ca^{2+}]_i$ elicited by depolarization within a millisecond time scale [21–23].

A change of $[Ca^{2+}]_i$ in the cytosolic compartment was represented as

$$\frac{d[Ca^{2+}]_i}{dt} = R_{Cyt} = R_{Buf} + R_{Loss} + R_{In} + R_{SERCA} + R_{CICR} + R_{ER,Leak}, \quad (1)$$

where the terms on the right side describe rates of the $[Ca^{2+}]_i$ change due to buffering, Ca^{2+} loss because of extrusion across the PM and diffusion, calcium influx into the cytosol, CICR, and Ca^{2+} leakage from the ER.

The rate of change in the $[Ca^{2+}]_i$ due to Ca^{2+} influx is defined as

$$\left(\frac{d[Ca^{2+}]}{dt}\right)_{In} = \frac{I_{Ca}}{2FV_{Cyt}} = R_{in},$$

where I_{Ca} is the calcium current through voltage-dependent channels, V_{Cyt} is the cytosolic volume, and F is the Faraday constant. The depolarization-induced Ca^{2+} current was described according to D'Angelo et al. [24]. The charge influx was calculated by integrating the current in time.

Removal of Ca^{2+} from an intracellular compartment attributable to pumping out across the PM and diffusion was calculated with the use of a first-order reaction

$$R_{Loss} = -P([Ca^{2+}]_i - [Ca^{2+}]_{i,rest}) = R_{Loss},$$

where P is the rate constant of Ca^{2+} removal, and $[Ca^{2+}]_{i,rest}$ is the resting $[Ca^{2+}]_i$. The R_{Loss} in our definition also includes a constant Ca^{2+} leak across the PM, which balances the Ca^{2+} removal at the resting Ca^{2+} concentration. We did not include Ca^{2+} influx into the cytosol through store-operated Ca^{2+} entry (SOCE). The process of SOCE activation is rather slow and requires at least several tens of seconds [25]; therefore, it was not suggested to affect Ca^{2+} transients within the time scale of our simulation.

Binding of Ca^{2+} to buffers was described as follows:

$$R_{Buf,Y} = -k_{fy}[Ca^{2+}]_i([TotalY] - [CaY]) + k_{by}[CaY], \quad \frac{d[CaY]}{dt} = -R_{Buf,Y},$$

where Y represents exogenous and endogenous buffers, $k_{f,y}$ and $k_{b,y}$ are the forward and backward binding rate constants, *[TotalY]* is the total buffer concentration, and *[CaY]* is the concentration of a Ca^{2+}-bound compound. A complete washout of mobile endogenous buffers typically occurs in whole-cell recordings. A Ca^{2+} indicator dye, Oregon Green 488 BAPTA-1 (OGB1), was included in the model. Since the concentration of the Ca^{2+}-bound indicator is proportional to the recorded intensity of single-wavelength fluorescence [26], it was used in some of our simulations to compare the recorded fluorescence changes and the model outcome.

The ER Ca^{2+} transport was described by Eqs. 2–5. The rate of Ca^{2+} uptake via SERCAs and CICR were simulated according to Albrecht et al. [18]. Since Ca^{2+}-dependent inactivation of CICR was suggested as one of the mechanisms of CICR termination [27], the inactivation variable h was included in some simulations:

$$R_{SERCA} = -\frac{v_{\max,SERCA}[Ca^{2+}]_i^N}{[Ca^{2+}]_i^N + K_{M,SERCA}^N} = R_{SERCA}, \quad (2)$$

$$R_{CICR} = k_{CICR}\frac{[Ca^{2+}]_i^M}{[Ca^{2+}]_i^M + K_{d,CICR}^M} h([Ca^{2+}]_{ER} - [Ca^{2+}]_i), \quad (3)$$

$$R_{ER,Leak} = k_{leak,ER}([Ca^{2+}]_{ER} - [Ca^{2+}]_i), \quad (4)$$

$$\frac{d[Ca^{2+}]_{ER}}{dt} = -\frac{R_{SERCA} + R_{ER,Leak} + R_{CICR}}{(1 + \frac{[TotalCRC]K_{d,CRC}}{(K_{d,CRC} + [Ca^{2+}]_{ER})^2}\frac{V_{ER}}{V_{Cyt}})} = -\frac{R_{ER}}{\kappa_{ER}}\frac{V_{ER}}{V_{Cyt}}, \quad (5)$$

where V_{ER} and V_{Cyt} are the ER and cytosolic volumes, $[Ca^{2+}]_{ER}$ is the free Ca^{2+} concentration in the ER, $k_{leak,ER}$ is the rate constant of the background Ca^{2+} leak across the ER membrane, $K_{d,CRC}$ is the dissociation constant of the ER Ca^{2+} buffer calreticulin, *[TotalCRC]* is the total concentration of the latter buffer, $v_{max,SERCA}$ is the maximum rate of SERCA, k_{CICR} is the rate constant of ER Ca^{2+} release due to CICR, $K_{M,SERCA}$ is the Michaelis constant, and N is the Hill coefficient for Ca^{2+} binding with SERCA. The $K_{d,CICR}$ is the dissociation constant for Ca^{2+} binding with RyRs, M is the Hill coefficient for Ca^{2+} binding with RyRs, and κ_{ER} is the ratio of a change in the total Ca^{2+} concentration to the accompanying change in the free Ca^{2+} concentration in the ER.

To take into consideration the mechanism of CICR inactivation, an additional equation was added to the system of Eqs. 1 and 5:

$$\frac{dh}{dt} = k_{b,h}(1-h) - k_{f,h}[Ca^{2+}]_i^{NH} h. \quad (6)$$

Here, $k_{b,h}$ and $k_{f,h}$ are the dissociation and association rate constants of Ca^{2+} binding with an inactivating site of the RyR channel, and NH is the Hill coefficient. The use of Hodgkin–Huxley

Table 1. Calcium Dynamics-Related Parameters

Parameter	Symbol	Standard value and limits	Refs
Calcium dynamics			
Initial cytosolic Ca^{2+} concentration	$[Ca^{2+}]_{i,rest}$	0.06 (0.03–0.1) μM	[15, 26]
Fixed buffer			
Total concentration	$[Buf]_T$	500 μM	[19, 29]
Dissociation constant	$K_{d,Buf}$	10 (5–10) μM	[30]
Forward binding rate constant	$k_{f,Buf}$	100 $\mu M^{-1}\cdot sec^{-1}$	[31]
Exogenous buffer OGB1			
Total concentration	$[OGB1]_T$	200 (10–200) μM	[10]
Dissociation constant	$K_{d,OGB1}$	0.2 (0.325) μM	[8]
Forward binding rate constant	$k_{f,OGB1}$	400 $\mu M^{-1}\cdot sec^{-1}$	[32]
Plasma membrane			
Rate constant of Ca^{2+} removal	P	214 (100–500) sec^{-1}	Fits to the experiment in [10]
Maximal Ca^{2+} conductance	$g_{max,Ca}$	$1.81\cdot10^{-5}$ $S\cdot cm^{-2}$	Fits to the experiment in [10]
Endoplasmic reticulum			
Initial Ca^{2+} concentration	$[Ca^{2+}]_{ER,rest}$	160 (100–400) μM	[18, 33, 34]
SERCA			
Michaelis–Menten constant	$K_{M,SERCA}$	0.04 μM*	[18]
Hill coefficient	N_{SERCA}	2.5	[18]
CICR			
Dissociation constant	$K_{D,CICR}$	2.641 μM	[18]
Hill coefficient	M_{CICR}	1.0	[18]
Calreticulin			
Total concentration	$[CRC]_T$	43 mM	[35–37]
Dissociation constant	$K_{d,CRC}$	2 mM	[35–37]

Footnotes: *In Albrecht et al. [18], $K_{M,SERCA}$ = 0.03 μM; in our model, $K_{M,SERCA}$ was set at 0.04 μM to provide a stable steady state at the resting $[Ca^{2+}]_i$ for the entire range of simulated parameters.

formalism allowed us to describe the inactivation process phenomenologically.

Simulations were performed using the NEURON simulation environment [28], and those will be available for download from the ModelDB database at http://senselab.med.yale.edu/modeldb/ after publication. All parameters of the model were selected as those for the room temperature. The parameter values are given in Table 1. To provide identical initial conditions for all simulations, we varied the model parameters $v_{max,SERCA}$ and k_{CICR}, adjusting the constant of the ER Ca^{2+} leak $k_{Leak,ER}$ in such a manner that the zero net flux across the ER membrane was obtained at rest.

RESULTS

We first examined whether a simple two-compartment model describing dynamic changes in the $[Ca^{2+}]_i$ and $[Ca^{2+}]_{ER}$ is sufficient to reproduce the effects of the prolonged preincubation of neurons with SERCA inhibitors that abolishes CICR. Any mechanisms of CICR termination besides of global depletion of the ER were not included in the model. To test the model behavior, we simulated Ca^{2+} transients elicited by 200-msec-long voltage-clamp depolarization from –70 to 0 mV at different values of the maximal rate of ER Ca^{2+} uptake ($v_{max,SERCA}$) and rate constant of Ca^{2+} release (k_{CICR}). These simulations started from identical steady-state initial conditions. We checked that a single equilibrium point of the system of ordinary differential equations

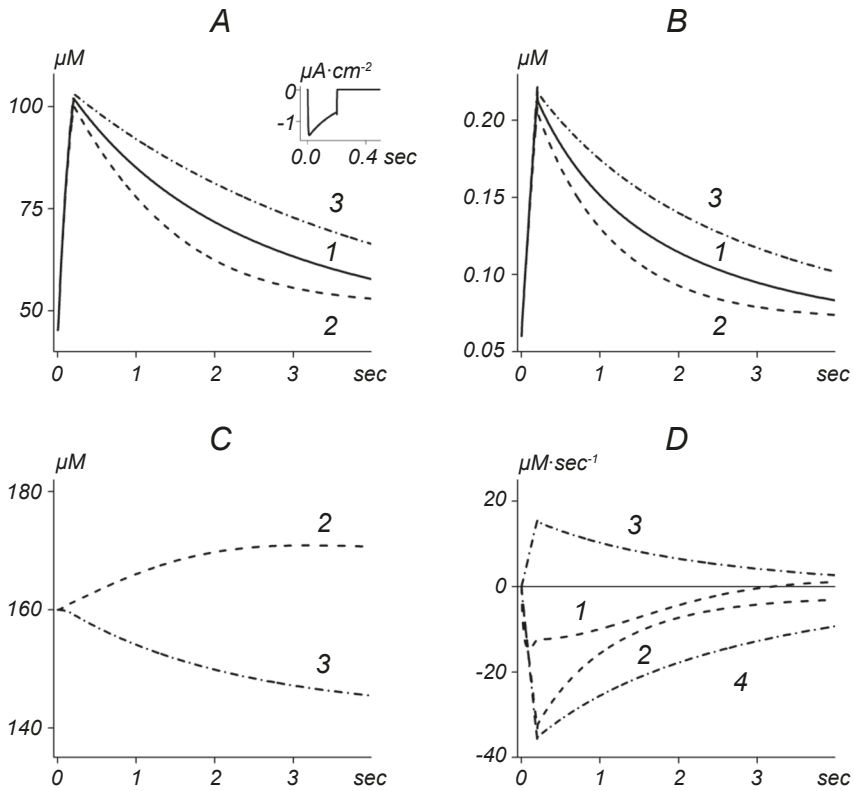

Fig. 1. Effects of SERCA inhibitors on Ca^{2+} transients in the models with net ER Ca^{2+} uptake and non-regenerative net ER Ca^{2+} release. A) Simulated changes in the concentration of OGB1, a Ca^{2+}-bound indicator ([CaOGB1]), B) those in the $[Ca^{2+}]_i$, and C) those in the $[Ca^{2+}]_{ER}$ after pretreatment with SERCA inhibitors (1), during net Ca^{2+} uptake by the ER (2), and during non-regenerative net Ca^{2+} release from the ER (3). In D), rates of changes in the $[Ca^{2+}]_i$ due to ER Ca^{2+} transport (R_{ER}, 1 and 3) and due to Ca^{2+} extrusion and diffusion (R_{Loss}, 2 and 4) are shown for the cases of net ER Ca^{2+} uptake (1 and 2) and non-regenerative net ER Ca^{2+} release (3 and 4). The R_{loss} value was corrected by subtraction of the leak. The parameters of the model with net ER Ca^{2+} uptake, $v_{max,SERCA}$ = 80 μM·sec^{-1} and $v_{max,CICR}$ = 1 sec^{-1}. The parameters of the model with non-regenerative net ER Ca^{2+} release, $v_{max,SERCA}$ = 9.5 μM·sec^{-1} and $v_{max,CICR}$ = = 1.9 sec^{-1}. Other parameters are given in Methods and Table 1. In A), a half-decay time is 1.62 sec, 1.04 sec, and 2.60 sec for traces 1–3, respectively. Abscissa) Time, sec; ordinate) μM in A–C) and μM sec^{-1} in D). An inset in A) shows the calcium current in the model. Ordinate) Calcium current, μA·cm^{-2}; abscissa) time, sec.

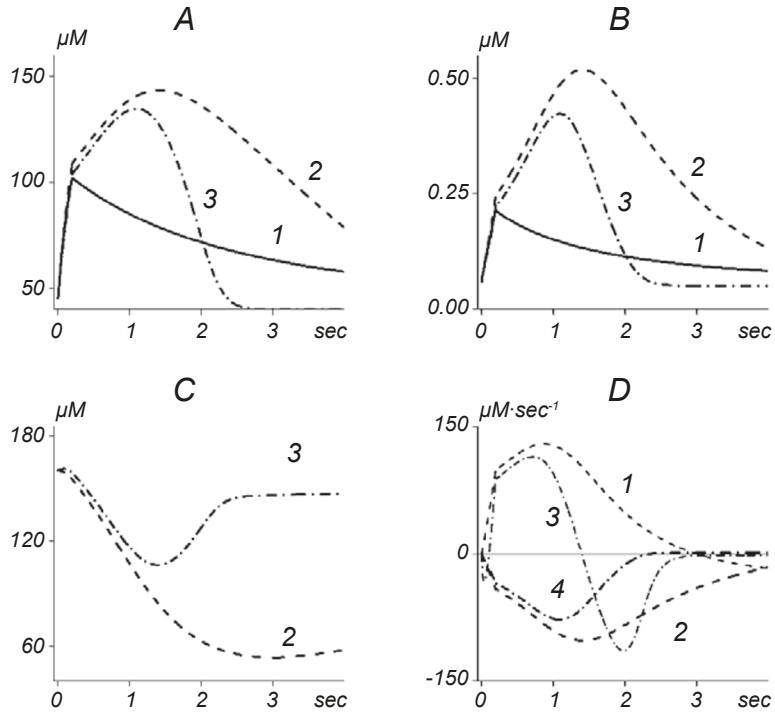

Fig. 2. Effects of SERCA inhibitors on Ca^{2+} transients in the models with regenerative net ER Ca^{2+} release. A) Simulated changes in the [CaOGB1], B) those in the $[Ca^{2+}]_i$, and C) those in the $[Ca^{2+}]_{ER}$ shown after pretreatment with SERCA inhibitors (1) and for the cases of regenerative net Ca^{2+} release from the ER, which resulted in a decreased (2) or increased (3) half-decay time ($t_{1/2}$) after application of the inhibitors. In D), rates of the changes in $[Ca^{2+}]_i$ due to ER Ca^{2+} transport (R_{ER}, 1 and 3) and due to Ca^{2+} extrusion and diffusion (R_{Loss}, 2 and 4) are shown for cases of the decreasing (1 and 2) or increasing (3 and 4) $t_{1/2}$ after application of the inhibitors. The parameters of the model with regenerative net Ca^{2+} release and increased half-decay time in the absence of CICR, $v_{max,SERCA}$ = = 510 μM·sec^{-1} and k_{CICR} = 2.5 sec^{-1}. The parameters of the model with regenerative net Ca^{2+} release and a decreased half-decay in the absence of CICR, $v_{max,SERCA}$ = 60 μM·sec^{-1}, and k_{CICR} = 1.1 sec^{-1}. Other parameters are given in Methods and Table 1. In A), $t_{1/2}$ = 1.62 sec, 2.05 sec, and 0.75 sec for traces 1–3, respectively. Designations are the same as in Fig. 1.

was stable for all sets of the parameters examined of Eqs. 1 and 5. Here we show the results for initial $[Ca^{2+}]_i$ and $[Ca^{2+}]_{ER}$ equal to 60 nM and 160 nM, respectively, but the same qualitative predictions were obtained for other initial conditions remaining within physiological ranges (see Table 1).

For some parameter values, the peak of Ca^{2+} transient in our model occurred immediately after termination of the depolarizing step. As was shown earlier [17], this was observed when the rate of net Ca^{2+} release from the ER was lower than the rate of Ca^{2+} clearance from the cytosol, i.e., when $R_i < 0$ (Fig.1). Otherwise, the net Ca^{2+} flux from the ER increased in a regenerative manner ($R_i > 0$) to the point where the rate of Ca^{2+} extrusion across the PM became equal to the net Ca^{2+} flux from the ER, i.e., $R_i = 0$ (Fig. 2). At a relatively large value of the $v_{max,SERCA}$, as compared with k_{CICR}, elimination of the ER Ca^{2+} transport resulted in the slowing down of the decay of Ca^{2+} transients. In this case, net Ca^{2+} uptake ($R_{ER} < 0$) was observed (trace 2 in Fig. 1A, B, C) or Ca^{2+} release was followed by uptake Ca^{2+} during the decay phase of the $[Ca^{2+}]_i$ transient (trace 3 in Fig. 2A, B, C). At a relatively large value of the k_{CICR}, as compared with $v_{max,SERCA}$, a net Ca^{2+} release ($R_{ER} > 0$) was observed (traces 3 in Fig. 1A, B, C and trace 2 in Fig. 2A, B, C), and elimination of the ER Ca^{2+} transport, resulted in acceleration of the decay of Ca^{2+} transients.

Any counteracting termination mechanism was not necessary for the termination of Ca^{2+} release in the model with a value of CICR gain smaller than a unity (as in Fig. 1). Simulated changes in the $[Ca^{2+}]_i$ were almost undistinguishable in models with fixed and dynamic $[Ca^{2+}]_{ER}$ (Fig. 3A, B). The ER Ca^{2+} release corresponded to a smoothly graded function of the trigger Ca^{2+} influx, which is seen from a perfectly linear dependence of the amplitude of the $[Ca^{2+}]_{ER}$ transient decrease ($\Delta[Ca^{2+}]_{ER}$) on the total charge carried by the Ca^{2+} current (Fig. 4A, trace 1). This release became non-linearly graded and then saturated at high levels of $[Ca^{2+}]_i$ because of saturation of the Ca^{2+} release mechanism. When net CICR had a regenerative phase (Fig. 2), it was still

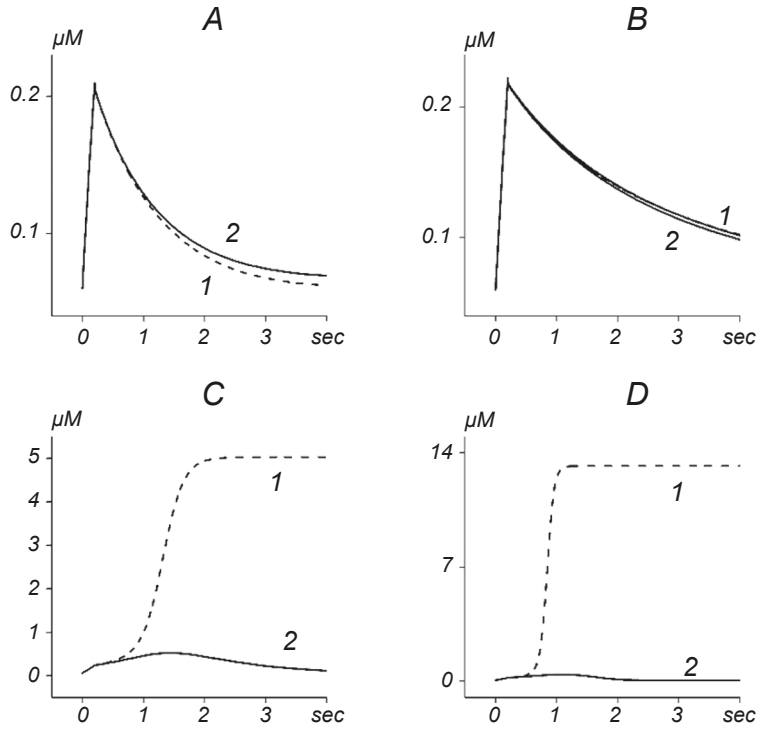

Fig. 3. Simulated Ca^{2+} transients in models with the fixed (1) and dynamic (2) ER Ca^{2+} concentration. Low-gain models in contrast to models with a high gain (> 1) do not require counteracting mechanisms for CICR termination. The parameters of the model in A), $v_{max,SERCA}$ = 80 μM·sec^{-1} and $v_{max,CICR}$ = 1 sec^{-1}, in B), $v_{max,SERCA}$ = 9.5 μM·sec^{-1} and $v_{max,CICR}$ = 1.9 sec^{-1}, in C), $v_{max,SERCA}$ = 60 μM·sec^{-1} and k_{CICR} = 1.1 sec^{-1}, and in D), $v_{max,SERCA}$ = 510 μM·sec^{-1} and k_{CICR} = 2.5 sec^{-1}. Other parameters are given in Methods and Table 1. Ordinate) Intracellular free calcium concentration, μM; abscissa) time, sec.

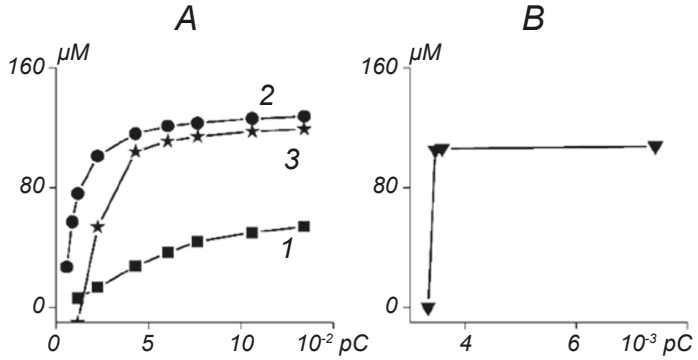

Fig. 4. Relationships between the charge carried by the Ca^{2+} current (abscissa, 10^{-2} and 10^{-3} pC in A) and B), respectively, and the amplitude of the $[Ca^{2+}]_{ER}$ decrease (ordinate, μM). A) Smoothly and non-linearly graded Ca^{2+} release and B) all-or-none Ca^{2+} release. For a 200-msec-long depolarizing step, the transition to all-or-none behavior occurs at the $g_{max,Ca}$ = 2,7·10^{-6} S·cm^{-2}. The parameters of ER Ca^{2+} transport, $v_{max,SERCA}$ = 9.5 μM·sec^{-1} and k_{CICR} = 1.9 sec^{-1} for trace 1 in A), 60 μM·sec^{-1} and k_{CICR} = 11 sec^{-1} for trace 2 in A), and 510 μM·sec^{-1} and k_{CICR} = 25 sec^{-1} for trace 3 in A) and B), respectively. In B), a fluorescent dye was not included in the model. Other parameters are given in Methods and Table 1.

graded by Ca^{2+} entry. Thus, a two-fold increase in the charge for values of the parameters (as for trace 3 in Fig. 2A) resulted in a 90% greater $\Delta[Ca^{2+}]_{ER}$ (104 μM vs. 54 μM; trace 3 in Fig. 4A). These simulations indicate that the regenerative (self-reinforcing) mode of net CICR does not preclude it from increasing in a graded manner with an increasing stimulus strength. In other words, regenerative CICR can be graded owing to the interplay between Ca^{2+} fluxes influenced by counteracting termination mechanisms. This gradation, however, is not strictly linear. Further increases in the maximal Ca^{2+} conductance ($g_{max,Ca}$) or duration of the depolarizing pulse resulted

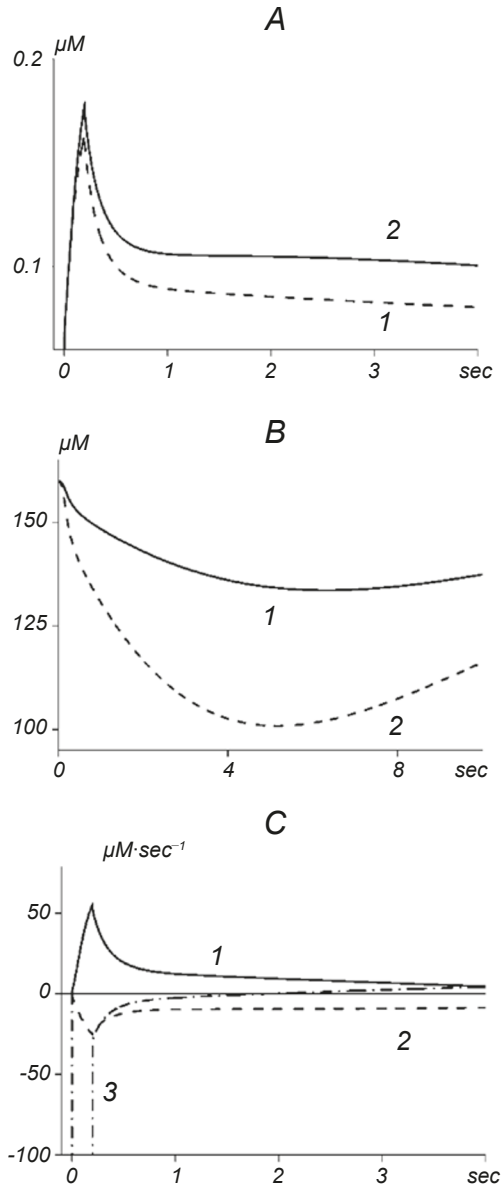

Fig. 5. Effects of slow Ca^{2+} buffers on the modes of net ER Ca^{2+} transport. In the presence of parvalbumin instead of a low-affinity endogenous buffer, as in Fig. 1B, the time to peak of the Ca^{2+} transient and the character of CICR are significantly determined by the rate of $[Ca^{2+}]_i$ change due to buffering. Ordinate in A), changes in the $[Ca^{2+}]_i$, μM; that in B), changes in the $[Ca^{2+}]_{ER}$ elicited by different Ca^{2+} influxes, μM, and that in C), rates of change of $[Ca^{2+}]_i$ due to ER Ca^{2+} transport (R_{ER}, 1), Ca^{2+} extrusion and diffusion (R_{Loss}, 2), and buffering (R_{Buf}, 3); ordinate, μM·sec^{-1}. The R_{loss} value was corrected by subtraction of the leak. The parameters of ER Ca^{2+} transport are the following: $v_{max,SERCA}$ = = 60 μM·sec^{-1} and k_{CICR} = 11 sec^{-1}. Parvalbumin was modeled with the apparent forward binding rate constant $k_{f,PV}$ = 5 μM^{-1}·sec^{-1} and dissociation constant $K_{d,Buf}$ = 0.2 μM [26]. Other parameters are given in Methods and Table 1. Abscissa) Time, sec.

in the almost complete saturation of the release mechanism by Ca^{2+} within the depolarizing step (Fig. 4A). When the $[Ca^{2+}]_{ER}$ in the model was fixed, a constant (all-or-none) Ca^{2+} release was observed (Fig. 3C, D), which is indicative of the importance of the termination mechanism. All-or-none Ca^{2+} release characterized by the same maximal $[Ca^{2+}]_i$ response at any higher-threshold strength of the stimulus could also be obtained in the model, e.g., when fluorescent dyes were not included (Fig. 4B).

Other parameters can also noticeably affect Ca^{2+} fluxes. Therefore, the transition between modes of CICR operation through regulation of the $[Ca^{2+}]_i$ and/or $[Ca^{2+}]_{ER}$ can be modified. Varying the value of the fractional ER volume within a plausible range (0.02−0.2 [23, 38]) resulted in a significant increase in the time to peak with increasing of the fractional volume in the models with regenerative net Ca^{2+} release. When the Hill coefficient M for Ca^{2+} binding with RyRs was increased in the model, non linear grading was observed for a narrower range of parameters, and saturation of RyRs occurred more quickly. This also allowed us to elicit a large increase in the $[Ca^{2+}]_i$ by introducing a small submicromolar Ca^{2+} concentration. Reducing the rate of Ca^{2+} removal from the cytosol (P) resulted in the model in transitions from the net ER Ca^{2+} uptake to non regenerative net ER Ca^{2+} release, from non-regenerative net Ca^{2+} release to non-linearly graded regenerative net Ca^{2+} release, and from non-linearly graded regenerative net Ca^{2+} release to steady-state Ca^{2+} oscillations.

Ca^{2+} fluxes across the ER and PM membranes are not the only players determining the mode of operation of the ER Ca^{2+} transport systems. Slow high-capacity buffers affect Ca^{2+} transients in a similar manner to calcium fluxes that remove Ca^{2+} from the cytosol, e.g., similarly to what is observed at the mitochondrial uptake. The replacement of a fast low-capacity buffer by a buffer with the properties of parvalbumin (Fig. 2) resulted in the model in the transition from regenerative net CICR to non-regenerative and smoothly graded net CICR (Fig. 5). This effect showed no dependence on the affinity of the buffer. In contrast, R_{Buf} is always zero at the peak of Ca^{2+} transient if only fast buffers were included in the model (Fig. 6D).

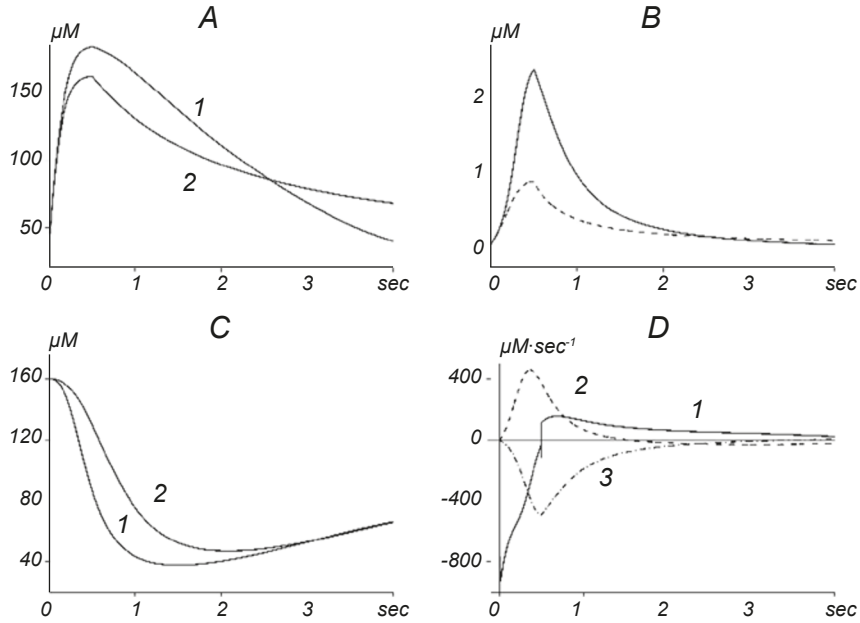

Fig. 6. Effects of stimulation conditions on the modes of net ER Ca^{2+} transport. A and B) Changes: in [CaOGB1] (A), in the $[Ca^{2+}]_i$ (B) with and without CICR (1 and 2 respectively). C) Changes in the $[Ca^{2+}]_{ER}$ elicited by different Ca^{2+} influxes; $g_{max,Ca}$ = 3.62·10^{-5} S·cm^{-2} (1) and $g_{max,Ca}$ = 1.81·10^{-5} S·cm^{-2} (2). D) Rates of changes in the $[Ca^{2+}]_i$ due to buffering (R_{Buf}, 1), ER Ca^{2+} transport (R_{ER}, 2), and Ca^{2+} extrusion and diffusion (R_{Loss}, 3$_s$). Parameters of the model, $v_{max,SERCA}$ = 60 μM·sec^{-1}, k_{CICR} = 11 sec^{-1}, and $g_{max,Ca}$ = 3.62·10^{-5} S·cm^{-2}. Depolarizing pulses are 500 msec long. Other parameters are given in Methods and Table 1. Designations are the same as in Fig.1.

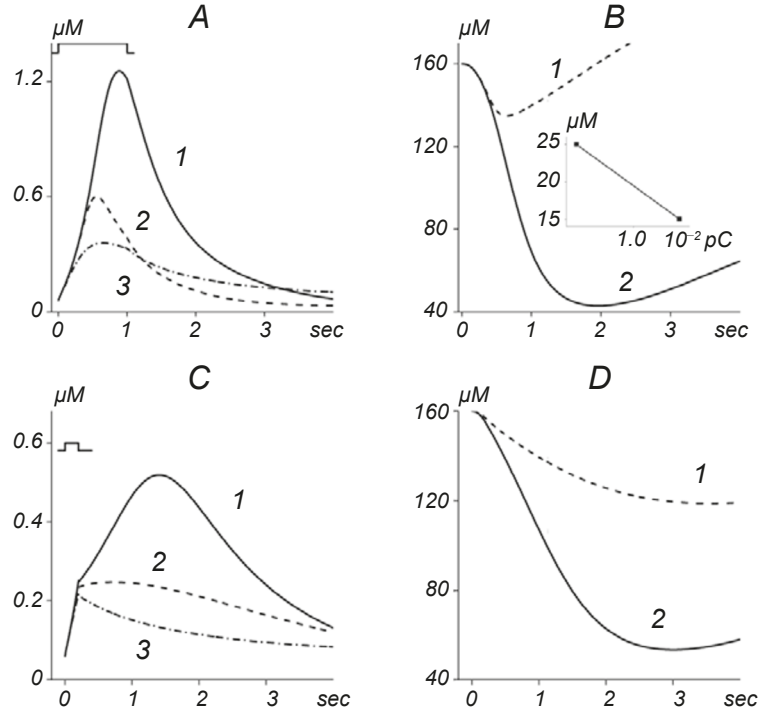

Fig. 7. Effects of CICR inactivation on the Ca^{2+} transients. A) and B), $[Ca^{2+}]_i$ and $[Ca^{2+}]_{ER}$ changes respectively (ordinate, μM) in the model with Ca^{2+}-dependent inactivation of CICR added. In an inset of B), relationships between the charge carried by the Ca^{2+} current (abscissa, 10^{-2} pC) and the amplitude of the $[Ca^{2+}]_{ER}$ decrease (ordinate, μM). The association and dissociation rate constants of Ca^{2+} binding with the inactivation site of RyRs and the Hill coefficient are $k_{f,h}$ = 50 μM^4·sec^{-1}, $k_{b,h}$ = 0.05 sec^{-1}, and NH = 4 in A) and B) respectively. The $k_{f,h}$ = 13 μM^{-1}·sec^{-1}, $k_{b,h}$ = 6.5 sec^{-1}, and NH = 1 in C) and D). In A–D), $v_{max,SERCA}$ = 60 μM·sec^{-1} and k_{CICR} = 11 sec^{-1}. Depolarizing pulses are 1 sec long in A) and 200 msec long in B). Other parameters are given in Methods and Table 1. Abscissa) Time, sec.

To evaluate different putative mechanisms that may be responsible for the interruption of positive feedback of CICR in neurons, we examined the effects of Ca^{2+}-dependent inactivation of CICR in our model (Eqs. 3 and 6). This resulted in a significantly smaller decrease in the $[Ca^{2+}]_{ER}$ and in a shorter time to peak of the $[Ca^{2+}]_i$ transient than in the model with the ER depletion as the only termination mechanism (Fig. 7). For some sets of the parameters, a decrease in the $[Ca]_{ER}$ content was followed by a recovery phase, whereas the neuronal membrane remained depolarized (Fig. 7A, B). The presence of such a recovery phase observed in the experimental measurements can be indicative of a situation when Ca^{2+} release channels enter the inactivated state. However, in the absence of the recovery phase during depolarization (Fig. 7C, D), the contribution of Ca^{2+}-dependent inactivation of RyRs to the CICR termination cannot be ruled out.

DISCUSSION

Our simulations showed that the interplay between Ca^{2+} transport systems and Ca^{2+} buffers may completely determine the modes of operation of the ER Ca^{2+} transport systems. Albrecht et al. [17, 18] described previously three modes of net CICR in sympathetic neurons in the absence of stimulated Ca^{2+} entry, i.e., after the termination of stimulation and at a fixed $[Ca^{2+}]_{ER}$: i) attenuated net Ca^{2+} uptake ($R_{ER} < 0$), ii) graded net Ca^{2+} release ($R_{Cyt} < < 0$, $R_{ER} > 0$), and iii) regenerative net Ca^{2+} release ($R_{Cyt} > 0$, $R_{ER} > 0$). Our simulations indicated that net CICR may demonstrate regenerative behavior for some period of time until the rates of changes in the Ca^{2+} concentration due to Ca^{2+} fluxes and buffers are equilibrated but are graded by Ca^{2+} influx owing to counteracting termination mechanisms. On the other hand, non regenerative net Ca^{2+} release can be non linearly graded and saturated at higher values of $[Ca^{2+}]_i$. Thus, we propose to define the main modes of net ER Ca^{2+} transport as i) net Ca^{2+} uptake ($R_{ER} < 0$), ii) non regenerative net Ca^{2+} release ($R_{Cyt} < 0$, $R_{ER} > 0$), and iii) regenerative net Ca^{2+} release ($R_{Cyt} > 0$, $R_{ER} > 0$). The number of modes can be extended if we take into account gradation by the trigger current. Thus, it is possible to distinguish such different modes of the net ER Ca^{2+} transport: i) net Ca^{2+} uptake, ii) non regenerative smoothly graded net Ca^{2+} release, iii) non regenerative, non linearly graded net Ca^{2+} release, iv) regenerative graded net Ca^{2+} release, and v) all-or-none Ca^{2+} release.

Separation and characterization of experimentally measured Ca^{2+} fluxes in sympathetic neurons [18, 23] revealed that the apparent Ca^{2+} sensitivity of the uptake pathway is much higher than the sensitivity of the release pathway, and SERCA becomes close to saturation at nanomolar $[Ca^{2+}]_i$ values. Our simulations showed that smoothly graded non regenerative CICR can be obtained for any pair of $v_{max,SERCA}$ and $k_{CICR,}$ but a range of the Ca^{2+} levels at which it can be observed may vary from very wide (e.g., with the parameters shown in Fig. 1) to very narrow (e.g., with those shown in Fig. 2). At higher $[Ca^{2+}]_i$ levels, Ca^{2+} release becomes non-linearly graded and then saturated because of saturation of the ER permeability, which is determined by saturation of RyRs. These results are in line with the data of experimental measurements of the $[Ca^{2+}]_{ER}$ in dorsal root ganglion neurons, where Ca^{2+} release was saturated only at long Ca^{2+} pulses [4]. Low-gain amplification confers an intrinsic stability to CICR. Unlike cardiac cells where CICR with high-gain amplification cannot be described within the framework of a common pool model, the results of our simulations suggest that a common-pool mechanism may be sufficient for some neurons in which CICR develops relatively slowly to achieve moderate amplification of the Ca^{2+} transients and still be graded by Ca^{2+} entry. As defined by Stern [39], common-pool models are those in which the trigger Ca^{2+} and released Ca^{2+} fluxes are passed through a common cytosolic pool, and all RyRs are controlled by the whole-cell trigger Ca^{2+} current.

Besides Ca^{2+} transport systems, the mode of CICR depends on Ca^{2+} buffering. When the rapid buffer approximation is valid, Ca^{2+} binding to buffers is fast compared with changes in $[Ca^{2+}]_i$. Fast Ca^{2+} buffers influence the interaction between Ca^{2+} fluxes indirectly, through regulation of the Ca^{2+} level in the cytosol, and the equilibrium with Ca^{2+} is reached at a peak of the Ca^{2+} transient at the time moment when $R_{ER} + R_{Loss} + R_{Buf} + R_{Entry} = 0$. On the contrary, slow high-capacity buffers determine the time to peak of the Ca^{2+} transient in a similar manner to Ca^{2+} fluxes through the cell membranes. Slow buffers, such as parvalbumin, may be expressed in some neurons in very high concentrations. For example, cerebellar basket cells contain about 563 μM of parvalbumin, on average [40], whereas outer hair cells of the frog sacculus contain 2.0–3.5 mM of parvalbumin-β, a

buffer with two functional Ca^{2+}-binding sites [41].

Our simulations suggest that a simple common-pool model for a small neuronal compartment may be sufficient to reproduce results of the main experimental observations concerning the action of SERCA inhibitors on depolarization-induced Ca^{2+} transients in different neurons. Several dissimilar modes of the effect of SERCA were distinguished. We define here modes of the effects of SERCA inhibitors as qualitative changes in the amplitude, decay time, and time to peak of the Ca^{2+} transient after preincubation with the drugs. Modes of the net ER Ca^{2+} transport do not always coincide with modes of the effects of SERCA inhibitors. For example, the removal of CICR may decrease or increase the decay time of the Ca^{2+} transient characterized by regenerative net Ca^{2+} release (Fig. 2). Thus, the peak amplitude and the time to peak of AP-evoked Ca^{2+} transients in the spines and dendrites of CA1 pyramidal neurons remained unchanged after CPA treatment, whereas the decay time increased by 50% [8]. In the somata of Purkinje cells, TG and CPA provided similar effects [7]. These effects are consistent with the net ER Ca^{2+} uptake simulated in our model (Fig. 1A). In the dendritic endings of cerebellar GrCs, preincubation of slices with 0.5 μM TG resulted in a 42% decrease in the peak amplitude, a decrease in the time to peak, and a decrease in the half-decay time of fluorescence transients from 2.59 to 1.62 sec [10]. Similar effects of CPA and TG were described at mossy fiber presynaptic terminals in the rat hippocampus [12]. In both cases, the gain value was larger than unity. These effects are consistent with regenerative net Ca^{2+} release in our model (Fig. 2). The effects of SERCA inhibitors demonstrated in Fig. 6A were similar to those described in the dendrites of hippocampal CA1 neurons during and after 1-sec-long depolarization [11] and in the cell bodies of rod photoreceptors [13]. It is important that experiments on photoreceptors were performed in the presence of mitochondrial blockers. As our model does not include mitochondria, the modeling results could be most directly related to the experimental recordings obtained in the presence of inhibitors of mitochondrial Ca^{2+} transport.

However, some additional assumptions may be necessary to reproduce qualitatively the action of SERCA inhibitors. Such inhibitors usually decrease the peak amplitude of Ca^{2+} transients when net non-regenerative Ca^{2+} release is observed (in particular Sandler and Barbara and Hackney et al. [14, 41]). We were able to reproduce this effect of SERCA inhibitors either by including some additional mechanisms of CICR termination (Fig. 7), or assuming a low Ca^{2+} ER load and a large ER volume fraction (e.g., 90 μM and 0.2 respectively, as in Fig. 5B in Albrecht et al. [17]), or using models CICR was largely saturated by Ca^{2+} influx (Fig. 6). Moreover, a smoothly graded and high-gain CICR may significantly contribute to Ca^{2+} transients in some neurons (e.g., Cohen et al. [5]), which could not be described by our model.

Thus, it can be concluded that the simplest spatially homogeneous compartmental models allow researchers to reproduce a number of experimental observations of Ca^{2+} ER transport, such as effects of the drugs that abolish CICR. Such models can successfully describe low-gain CICR in neurons. Our simulations suggest that Ca^{2+} transients in some neuronal types may be modestly amplified by regenerative CICR, which is graded and self-limiting owing to the presence of counteracting termination mechanisms. However, such models have limitations for the description of both high-gain and smoothly graded Ca^{2+} release in neurons meets certain difficulties.

Acknowledgment. I would like to sincerely thank Dr. David Friel for his helpful comments and support.

This is a computer modeling study; thus, confirmation of its correspondence to the existing international ethical standards for the experimental works on animals and humans is not necessary.

The author, E. È. Saftenku, confirms the absence of any conflicts over commercial or financial relations or relations with organizations or individuals that could in any way be related to the study.

REFERENCES

1. O. H. Petersen, M. Michalak, and A. Verkhratsky, "Calcium signalling: past, present and future," *Cell Calcium*, **38**, No. 3–4, 161–169 (2005); doi: 10.1016/j.ceca.2005.06.023.
2. A. Verkhratsky, "Physiology and pathophysiology of the calcium store in the endoplasmic reticulum of neurons," *Physiol. Rev.*, **85**, No. 1, 201–279 (2005); doi: 10.1152/physrev.00004.2004.
3. D. D. Friel and R. W. Tsien, "A caffeine- and ryanodine-sensitive Ca^{2+} store in bullfrog sympathetic neurones modulates effects of Ca^{2+} entry on $[Ca^{2+}]_i$," *J. Physiol.*, **450**, 217–246 (1992); doi: 10.1113/jphysiol.1992.sp019125.

4. N. Solovyova, N. Veselovsky, E. C. Toescu, and A. Verkhratsky, "Ca^{2+} dynamics in the lumen of the endoplasmic reticulum in sensory neurons: direct visualization of Ca^{2+}-induced Ca^{2+} release triggered by physiological Ca^{2+} entry," *EMBO J.,* **21**, No. 4, 622−630 (2002); doi: 10.1093/emboj/21.4.622.
5. A. S. Cohen, K. A. Moore, R. Bangalore, et al., "Ca^{2+}-induced Ca^{2+} release mediates Ca^{2+} transients evoked by single action potentials in rabbit vagal afferent neurones," *J. Physiol.*, **499**, Pt. 2, 315−328 (1997); doi: 10.1113/jphysiol.1997.sp021929.
6. Y. M. Usachev and S. A. Thayer, "All-or-none Ca^{2+} release from intracellular stores triggered by Ca^{2+} influx through voltage-gated Ca^{2+} channels in rat sensory neurons," *J. Neurosci.*, **17**, No. 19, 7404−7414 (1997); doi: 10.1523/JNEUROSCI.17-19-07404.1997.
7. L. Fierro, R. DiPolo, and L. Llano, "Intracellular calcium clearance in Purkinje cell somata from rat cerebellar slices," *J. Physiol.* **510**, Pt. 2, 499−512 (1998); doi: 10.1111/j.1469-7793.1998.499bk.x.
8. B. L. Sabatini, T. G. Oertner, and K. Svoboda, "The life cycle of Ca^{2+} ions in dendritic spines," *Neuron*, **33**, No. 3, 439–452 (2002); doi: 10.1016/s0896-6273(02)00573-1.
9. T. Akita and K. Kuba, "Functional triads consisting of ryanodine receptors, Ca^{2+} channels, and Ca^{2+}-activated K^+ channels in bullfrog sympathetic neurons. Plastic modulation of action potential," *J. Gen. Physiol.*, **116**, No. 5, 697−720 (2000); doi: 10.1085/jgp.116.5.697.
10. D. Gall, F. Prestori, E. Sola, et al., "Intracellular calcium regulation by burst discharge determines bidirectional long-term synaptic plasticity at the cerebellum input stage," *J. Neurosci*., **25**, No. 19, 4813–4822 (2005); doi: 10.1523/JNEUROSCI.0410-05.2005.
11. S. Alford, B. G. Frenguelli, J. G. Schofield, and G. L. Collingridge, "Characterization of Ca^{2+} signals induced in hippocampal CA1 neurons by the synaptic activation of NMDA receptors," *J. Physiol.*, **469**, 693–716 (1993); doi: 10.1113/jphysiol.1993.sp019838.
12. Y. Liang, L. L. Yuan, D. Johnston, and R. Gray, "Calcium signaling at single mossy fiber presynaptic terminals in the rat hippocampus," *J. Neurophysiol.,* **87**, No. 2, 1132−1137 (2002); doi: 10.1152/jn.00661.2001.
13. T. Szikra and D. Križaj, "Intracellular organelles and calcium homeostasis in rods and cones," *Vis. Neurosci*., **24**, No. 5, 733−743 (2007); doi: 10.1017/S0952523807070587.
14. V. M. Sandler and J. G. Barbara, "Calcium-induced calcium release contributes to action-potential evoked calcium transients in hippocampal CA_1 pyramidal neurons," *J. Neurosci.*, **19**, No. 11, 4325–4336 (1999); doi: 10.1523/JNEUROSCI.19-11-04325.1999.
15. F. Helmchen, K. Imoto, and B. Sakmann, "Ca^{2+} buffering and action potential-evoked Ca^{2+} signaling in dendrites of pyramidal neurons," *Biophys. J.*, **70**, No. 2, 1069–1081 (1996); doi: 10.1016/S0006-3495(96)79653-4.
16. D. W. Tank, W. G. Regehr, and K. R. Delaney, "A quantitative analysis of presynaptic calcium dynamics that contribute to short-term enhancement," *J. Neurosci.*, **15**, No. 12, 7940–7952 (1995); doi: 10.1523/JNEUROSCI.15-12-07940.1995.
17. M. A. Albrecht, S. L. Colegrove, J. Hongpaisan, et al., "Multiple modes of calcium-induced calcium release in sympathetic neurons I: attenuation of endoplasmic reticulum Ca^{2+} accumulation at low $[Ca^{2+}]_i$ during weak depolarization," *J. Gen. Physiol.*, **118**, No. 1, 83−100 (2001); doi: 10.1085/jgp.118.1.83.
18. M. A. Albrecht, S. L. Colegrove, and D. D. Friel, "Differential regulation of ER Ca^{2+} uptake and release rates accounts for multiple modes of Ca^{2+}-induced Ca^{2+} release," *J. Gen. Physiol.*, **119**, No. 3, 211–233 (2002); doi: 10.1085/jgp.20028484.
19. S. D. Brenowitz and W. G. Regehr, "Reliability and heterogeneity of calcium signaling at single presynaptic boutons of cerebellar granule cells," *J. Neurosci.*, **27**, No. 30, 7888–7898 (2007); doi: 10.1523/JNEUROSCI.1064-07.2007.
20. S. L. Colegrove, M. A. Albrecht, and D. D. Friel, "Quantitative analysis of mitochondrial Ca^{2+} uptake and release pathways in sympathetic neurons. Reconstruction of the recovery after depolarization-evoked $[Ca^{2+}]_i$ elevations," *J. Gen. Physiol.*, **115**, No. 3, 371–388 (2000); doi: 10.1085/jgp.115.3.371.
21. T. Xu, M. Naraghi, H. Kang, and E Neher, "Kinetic studies of Ca^{2+} binding and Ca^{2+} clearance in the cytosol of adrenal chromaffin cells," *Biophys. J.*, **73**, No. 1, 532–545 (1997); doi: 10.1016/S0006-3495(97)78091-3.
22. M.-H. Kim, N. Korogod, R. Schneggenburger, et al. "Interplay between Na^+/Ca^{2+} exchangers and mitochondria in Ca^{2+} clearance at the calyx of Held," *J. Neurosci.,* **25**, No. 26, 6057−6065 (2005); doi: 10.1523/JNEUROSCI.0454-05.2005.
23. M. Patterson, J. Sneyd, and D. D. Friel, "Depolarization-induced calcium responses in sympathetic neurons: relative contributions from Ca^{2+} entry, extrusion, ER/mitochondrial Ca^{2+} uptake and release, and Ca^{2+} buffering," *J. Gen. Physiol.*, **129**, No. 1, 29−56 (2007); doi: 10.1085/jgp.200609660.
24. E. D'Angelo, T. Nieus, A. Maffei, et al. "Theta-frequency bursting and resonance in cerebellar granule cells: experimental evidence and modeling of a slow K^+-dependent mechanism," *J. Neurosci.*, **21**, No. 3, 759–770 (2001); doi: 10.1523/JNEUROSCI.21-03-00759.2001.
25. J. Liou, M. Fivaz, T. Inoue, and T. Meyer, "Live-cell imaging reveals sequential oligomerization and local plasma membrane targeting of stromal interaction molecule 1 after Ca^{2+} store depletion," *Proc. Natl. Acad. Sci. USA,* **104**, No. 22, 9301−9306 (2007); doi: 10.1073/pnas.0702866104.
26. M. Maravall, Z. F. Mainen, B. L. Sabatini, and K Svoboda, "Estimating intracellular calcium concentrations and buffering without wavelength rationing," *Biophys. J.,* **78**, No. 5, 2655−2667 (2000); doi: 10.1016/S0006-3495(00)76809-3.
27. T. Akita and K. Kuba, "Ca^{2+}-dependent inactivation of Ca^{2+}-induced Ca^{2+} release in bullfrog sympathetic neurons," *J. Physiol.*, **586**, 3365−3384 (2008); doi: 10.1113/jphysiol.2008.153833.

28. M. L. Hines and N. T. Carnevale, "The NEURON simulation environment," *Neural Comput.,* **9**, No. 6, 1179–1209 (1997); doi: 10.1162/neco.1997.9.6.1179.
29. F. Helmchen and D. W. Tank, "A single-compartment model of calcium dynamics in nerve terminals and dendrites," *Cold Spring Harb. Protoc.*, **2015**, No. 2, 155−167 (2015); doi: 10.1101/pdb.top085910.
30. J. Klingauf and E. Neher, "Modeling buffered Ca^{2+} diffusion near the membrane: implications for secretion in neuroendocrine cells," *Biophys. J.* **72**, No. 2, Pt. 1, 674–690 (1997); doi: 10.1016/s0006-3495(97)78704-6.
31. S. P. Robertson, J. D. Johnson, and J. D. Potter, "The time course of Ca^{2+} exchange with calmodulin, troponin, parvalbumin, and myosin in response to transient increases in Ca^{2+}," *Biophys. J.*, **34**, No. 3, 559–569 (1981); doi: 10.1016/S0006-3495(81)84868-0.
32. M. Naraghi and E. Neher, "Linearized buffered Ca^{2+} diffusion in microdomains and its implications for calculation of $[Ca^{2+}]$ at the mouth of a calcium channel," *J. Neurosci.*, **17**, No. 18, 6961–6973 (1997); doi: 10.1523/JNEUROSCI.17-18-06961.1997.
33. M.T. Alonso, M. J. Barrero, E. Carnicero, et al., "Functional measurements of $[Ca^{2+}]$ in the endoplasmic reticulum using a herpes virus to deliver targeted aequorin," *Cell Calcium*, **24**, No. 2, 87−96 (1998); doi: 10.1016/s0143-4160(98)90076-8.
34. A. Miyawaki, J. Lopis, R. Heim, et al., "Fluorescent indicators for Ca^{2+} based on green fluorescent proteins and calmodulin", *Nature*, **388**, No. 6645, 882−887 (1997); doi: 10.1038/42264.
35. K. H. Krause and M. Michalak, "Calreticulin," *Cell*, **88**, No. 4, 439–443 (1997); doi: 10.1016/s0092-8674(00)81884-x.
36. H. Mogami, J. Gardner, O. V. Gerasimenko, et al., "Calcium binding capacity of the cytosol and endoplasmic reticulum of mouse pancreatic acinar cells", *J. Physiol.*, **518**, Pt. 2, 463–467 (1999); doi: 10.1111/j.1469-7793.1999.0463p.x.
37. M. M. Wu, M Grabe, S. Adams, et al., "Mechanisms of pH regulation and the regulated secretory pathway," *J. Biol. Chem.*, **276**, No. 35, 33027–33035 (2001); doi: 10.1074/jbc.M103917200.
38. E. De Schutter and P. Smolen, "Calcium dynamics in large neuronal models", in: *Methods in Neuronal Modeling: from Ions to Networks*, C. Koch and I. Segev (Eds.), 2nd ed., MIT Press, Cambridge (1998), pp. 211−250.
39. M. D. Stern, "Theory of excitation–contraction coupling in cardiac muscle," *Biophys J.*, **63**, No. 2, 497−517 (1992); doi: 10.1016/S0006-3495(92)81615-6.
40. E. Eggermann and P. Jonas, "How the 'slow' Ca^{2+} buffer parvalbumin affects transmitter release in nanodomain-coupling regimes," *Nat. Neurosci.*, **15**, No. 1, 20–22 (2011); doi: 10.1038/nn.3002.
41. C. M. Hackney, S. Mahendrasingam, A. Penn, and R. Fettiplace, "The concentrations of calcium buffering proteins in mammalian cochlear hair cells", *J. Neurosci.*, **25**, No. 34, 7867–7875 (2005); doi: 10.1523/JNEUROSCI.1196-05.2005.